Dou, Jinze; Vuorinen, Tapani; Koivula, Hanna; Forsman, Nina; Sipponen, Mika; Hietala, Sami

# Self-Standing Lignin-Containing Willow Bark Nanocellulose Films for Oxygen Blocking and UV Shielding

*Published in:*
ACS Applied Nano Materials

*DOI:*
10.1021/acsanm.1c00071

Published: 26/03/2021

*Document Version*
Publisher's PDF, also known as Version of record

ACS APPLIED NANO MATERIALS

www.acsanm.org

Article

# Self-Standing Lignin-Containing Willow Bark Nanocellulose Films for Oxygen Blocking and UV Shielding

Jinze Dou,* Tapani Vuorinen, Hanna Koivula, Nina Forsman, Mika Sipponen, and Sami Hietala

Cite This: *ACS Appl. Nano Mater.* 2021, 4, 2921−2929

Read Online

ACCESS | Metrics & More | Article Recommendations | Supporting Information

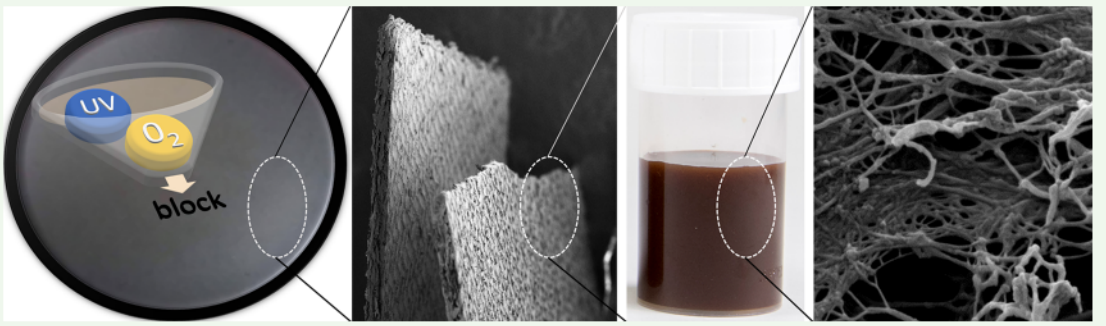


**ABSTRACT:** Developing the bio-based barrier material to substitute the petroleum-based one is the trend in functional packaging applications. Utilization of the abundantly underappreciated bark biomass is attractive from the sustainability point of view; however, an upgraded approach is required to maximize the performances of the lignin-containing cellulose nanofibril (LCNF) films from willow bark. Herein, hot water extraction (HWE) and microfluidization were studied for their effect on the yield of LCNF and its film performance after treatment of aqueous *p*-toluenesulfonic acid. The resultant HWE films were superior to the nontreated ones regarding yield, moisture, and oxygen barrier properties. In particular, the HWE films achieved an oxygen permeability of 3 $cm^3 \cdot \mu m/m^2 \cdot kPa \cdot day$ at 50% relative humidity, which is among the lowest achieved for single bio-based materials and comparable to commercially available synthetic barrier films. The LCNF films attained complete blocking of UV light transmission within the wavelength range of 290−400 nm. Overall, this study shows that HWE pretreatment not only allows the recovery of high-value extracts, but also significantly improves the yield of LCNF and its barrier performances. The biocompatible, lignin-containing, and self-standing hydrophobic nanocellulose films show promise as a barrier layer against UV radiation and oxygen permeation in food packaging and other applications.

**KEYWORDS:** *food packaging, lignin-containing, oxygen barrier, ultraviolet, water pretreatment, willow bark*



## INTRODUCTION

Approximately one-third (roughly 1.3 billion tons) of all edible food produced for human consumption is wasted annually in the world,[1] which equals to a significant squandering of natural and human resources from a global perspective in planting, harvesting, and transporting. Although there is no established correlation between shelf life and food spoilage, food packaging has gained considerable attention in preventing food waste by maintaining quality to prolong the shelf life of food and beverages.[2] Although plastic packaging has gradually replaced the traditional glass and metal packaging because of its advantages regarding weight, cost, and flexibility in design, plastics often suffer from poor barrier protection against oxygen and light.[2]

For instance, the cost-efficient artificial fluorescent lighting system that is favored by the retailers has high quantum energy due to its bands between 315 and 365 nm, which can extract protons from protein- or fat-based food. The photosensitizer-induced photo-oxidation can be easily activated especially in the presence of oxygen[3] and may cause irreversible loss of nutritional values and taste[4] and possibly enhance the formation of undesirable odors and flavors.[5] As known, photon energy is inversely proportional to the wavelength of the light source according to the Planck−Einstein relation. Therefore, the ultraviolet (UV) band (100−400 nm) carries a higher energy than visible light (400−700 nm) and can activate a higher rate of photo-oxidation.[6] In other words, the rate of photo-oxidation depends primarily on the presence of both oxygen and UV light. On the other hand, there has been an emerging trend to shift from petroleum-based polymeric

Received: January 9, 2021
Accepted: February 16, 2021
Published: February 26, 2021

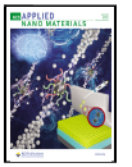

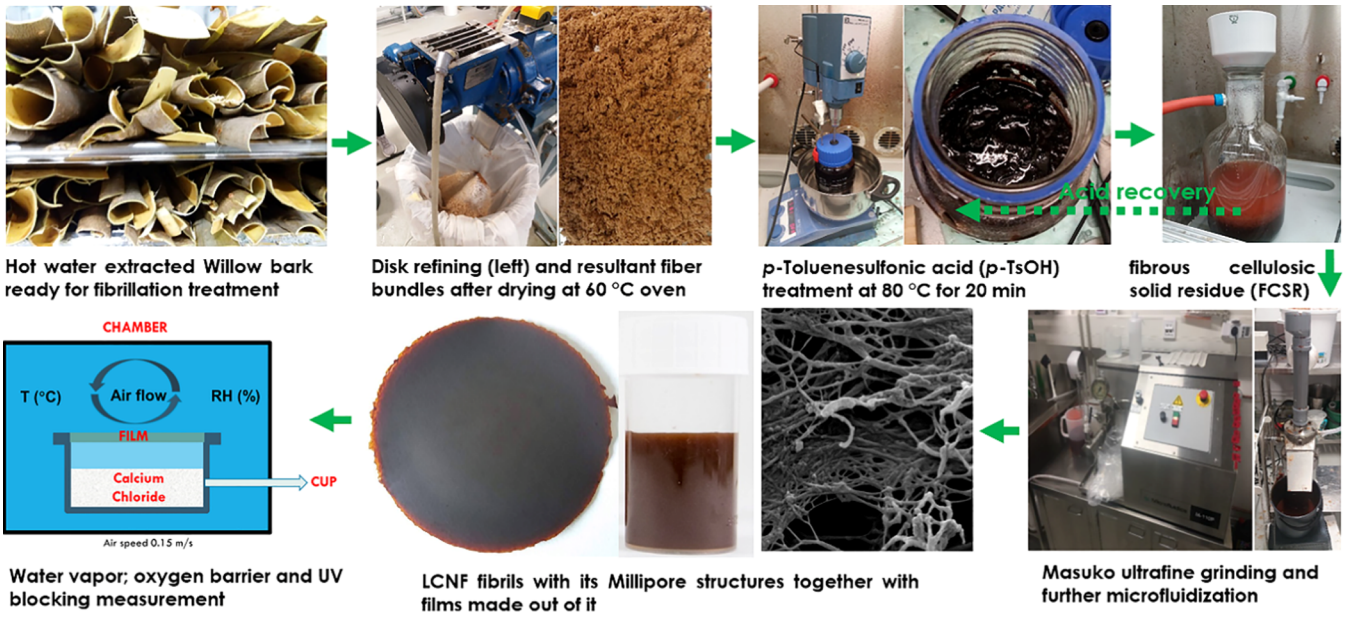


**Figure 1.** Experimental flow of fabricating lignin-containing cellulose nanofibrils (LCNF) and LCNF films from hot water-extracted willow bark (HWEWB), using a recyclable acid hydrotrope (*p*-TsOH).

matrices towards more environmentally friendly cellulose-based materials.[7]

In this regard, development of UV-shielding films or filters for food packaging is significantly required to block the transmission of the energetic UV radiation, i.e., the regions of UVB (290−320 nm) and UVA (320−400 nm). Incorporating UV light absorbers like inorganic metal oxides (e.g., nanosized titanium dioxide and zinc oxide),[8] organic compounds (e.g., salicylates and cyanoacrylates), hybrid compounds (e.g., hydroxyl benzophenone blended with silicon alkoxides),[4] and natural light absorbers (e.g., betel extract)[9] into the polymeric material can increase its absorption efficacy against natural or artificial UV light. Although the deterioration of the food can be significantly reduced, there remains the risk that UV absorbers can migrate into the food and may cause carcinogenic effects on human health.[10,11] The polymer photostabilization can also be strengthened by introducing stabilizers, such as excited-state quenchers, peroxide decomposers, and free radical scavengers.[12]

Minimizing or blocking oxygen permeation through the package is another key factor to prevent the rate of photo-oxidation. Nanocellulose has been known for its features such as high surface area and dense nanofibril network structure, which allow its use as an oxygen barrier layer for food packaging.[7] The major disadvantage is that the nanofibril can interact with the water molecules because of its associated hydroxyl groups, which can cause unwanted physical deformation in an atmosphere of oxygen and water. Reported approaches have been taken to improve the oxygen barrier performance of nanocellulose by tuning its crystallinity or introducing functional hydrophobic groups (like the alkyl type), which includes the oxidation pretreatments (e.g., TEMPO-catalyzed oxidation,[13] regioselective oxidative,[14] and butylamino-functionalization[15]), surfactant adsorption,[16] and polymer grafting.[17]

Therefore, engineering the nanocellulose-based thin film as a barrier layer inside the food package can help in preserving the freshness of food and beverages by blocking external oxygen and UV light. The inherent dark color of the willow bark (WB) fibril films,[18] along with other intriguing features, e.g., low moisture sorption behavior, high hydrophobicity, and richness of phenol-type compounds, inspired us to investigate especially the oxygen and UV-blocking performance of such nanocellulose films. Hence, an in-depth analysis of water vapor, oxygen barrier, and the UV-blocking performance of willow bark fibril films was executed. In addition, the effects of hot water extraction (HWE) and microfluidization were investigated here for achieving a complete valorization of the willow bark.

## EXPERIMENTAL SECTION

**Materials and Chemicals.** All chemicals and solvents were used as supplied from Sigma-Aldrich unless described elsewhere. The four-year-old willow hybrid "Karin" (SalixEnergi Europa AB) was harvested from the plantation site of the VTT Technical Research Center of Finland located in Kyyjärvi on May 13, 2015 and immediately transferred to a −20 °C freezer to keep it fresh. The bark was stripped off manually and cut into 2 cm pieces before keeping it at room temperature until further use. The microfibrillated cellulose (MFC) was prepared from bleached Kraft pulp (mixture of pine and spruce) using the Masuko supermass colloider (MKZA10-15J, Japan) and was used as a reference sample.

**Experimental Flow.** Hot water extraction (HWE) of the bark was performed at 80 °C for 30 min (Figure 1). Both the HWE-treated and nontreated bark were processed in a disk refiner to obtain coarse fiber bundles (FBs) before introducing them into aqueous 60 wt % *p*-toluenesulfonic acid (*p*-TsOH) at a *p*-TsOH/FB ratio of 10:1 at 80 °C for a period of 20 min to liberate the fibrous cellulosic solid residue (FCSR). The mechanisms involved catalysis of the dissolution or hydrolysis of carbohydrate and lignin through the ionized tosylate group ($pK_a$ for *p*-TsOH = −2.8 at 20 °C). Furthermore, *p*-TsOH could be simply extracted after the re-cycling of the hydrolysate due to its low water solubility.[19]

The dissolved high-molecular-weight (HMW) substances were precipitated by diluting the acid liquor with cold water below the lower concentration level required for the hydrotrope, followed by centrifugation and lyophilization for further analyses. FCSR was mechanically grinded by the supermass collider to avoid clogging of the microfluidizer (Microfluidic M-110P equipped with 1.5 kW


https://dx.doi.org/10.1021/acsanm.1c00071
ACS Appl. Nano Mater. 2021, 4, 2921−2929

Table 1. Yields of Klason Lignin and Proteins (% of the Original Mass) from the Willow Bark (WB) and Hot Water-Extracted Willow Bark (HWEWB) Together with the LCNF Obtained from Them[a]

| | WB | HWEWB | WB 6 | WB 12 | HWEWB 6 | HWEWB 12 |
|---|---|---|---|---|---|---|
| microfluidizer cycles | | | 6 | 12 | 6 | 12 |
| yield (%) | 100 | 100 | 55.1 | 55.1 | 67.1 | 67.1 |
| yield on original bark (%) | 100 | 78 | 55.1 | 55.1 | 52.3 | 52.3 |
| Klason lignin (%) | 17.3 | 20.8 | 32.4 | 29.4 | 34.5 | 30.7 |
| Klason lignin on original bark (%) | 17.3 | 16.4 | 17.6 | 16.0 | 18.3 | 16.2 |
| proteins (%) | 12.6 | 13.6 | 0.2 | 2.7 | 0.8 | 0 |
| proteins on original bark (%) | 12.6 | 11.0 | 0.1 | 1.5 | 0.4 | 0 |

[a]Reported data are mean values of two independent experiments. HWEWB refers to the hot water-extracted willow bark; WB 6 and WB 12 refer to LCNF prepared from the solid residues of willow bark with 6 and 12 rounds of microfluidization; HWEWB 6 and HWEWB 12 refer to LCNF prepared from the solid residues of the hot water-extracted willow bark with 6 and 12 rounds of microfluidization.

output) used for further fibrillation. Then, well-grinded FCSR fractions were continuously passed through the z-shaped chamber of the microfluidizer with the nozzle adjusted from 400 to 100 $\mu$m. The effect of defibrillation was controlled by adjusting the cycle numbers from 6[20] to 12. The lignin-containing cellulose nanofibrils (LCNF) were further fabricated into self-standing thin films using the combined slow filtration and hot pressing methods described earlier.[18] The Sefar Nitex polyamine monofilament (pore size: 10 $\mu$m) was used here to screen the 1% LCNF suspensions under the pressure of 2.5 bar. The LCNF film was then dried under room temperature for 4 min and then pressed for a further 2 h under a pressure of 1.8 kPa at 100 °C. Descriptive statistics was adopted in this study as the statistical method.

**Characterization.** *Chemical Analyses.* In order to eliminate their possible effects on lignin quantification, extractives, proteins, and tannins were removed from the samples (willow bark, LCNF) prior to the Klason lignin analysis (Figure S1, Supporting Information). The samples were first extracted with dichloromethane. The extracted samples were then mixed with 1% pepsin solution in 0.1 M HCl at a liquid/solid ratio of 25:1 and incubated by agitation at 37 °C for 16 h to eliminate proteins. The enzyme-treated samples were washed with hot water until neutrality was achieved. The protein content was defined as the weight loss in the pepsin treatment. Tannins were removed by further treatment with 0.1 M NaOH under nitrogen flow at 100 °C for 1 h.[21] The extracted protein- and tannin-free samples were analyzed for lignin and carbohydrates using NREL/TP-510-42618. The carbohydrate analysis was conducted using the high-performance anion-exchange chromatography (HPAEC) with pulsed amperometric detection (PAD) (Dionex ICS-3000, CarboPac PA 20 column, Sunnyvale, CA).

*Morphology and Tensile Test.* Zeiss Sigma VP was used to record the scanning electron microscopy (SEM) images on the morphological structures of LCNF and LCNF films. Sputter coating with platinum/palladium was used to increase the electric conductivity and avoid charging. SEM images were taken at 2 and 5 kV operating voltage for LCNF and LCNF films, respectively. The specimens were preconditioned at 23 °C and 50% relative humidity (RH). The tensile analysis was performed using an MTS 400/M Vertical Tensile Tester equipped with a 2 kN load cell according to ISO 527-1.[18]

*Atomic Force Microscopy (AFM) and Contact Angle.* Surface roughness and fibril thickness were measured using the AFM imaging technique on a Nanoscope V MultiMode scanning probe microscope (Bruker Corporation, Massachusetts). The radius of curvature from the tip was approximately less than 10 nm. The surface roughness parameters $R_q$ and $R_a$ were calculated on the basis of two or three image replicates.[22] Moreover, thickness distribution of the fibril was determined based on the AFM height measurement. The contact angles were characterized for the films under the CAM 200 (KSV Instruments Ltd., Helsinki, Finland). The detailed parameters were described previously.[18]

*Water Vapor Transmission Rate (WVTR).* The WVTR test was performed according to the ASTM E 96/E 96M−05 dessicant method with a minor modification. A preconditioning of samples was performed at 50% relative humidity (RH) as recommended by the standard. Results were calculated from three replicates. The dessicant-filled containers were covered with the sample and sealed mechanically from the edges. The containers were weighed and placed in the humidity-controlled chambers and weighed periodically. The RH gradient and temperature used in these measurements were 0/75% and 23 °C, respectively. The Rotronic RH meter (Bassersdorf, Switzerland) was adopted here for a systematic control of the cabinet temperature and RH prior to each weighing. The thickness of the specimen was determined using a micrometer (Lorentzen & Wettre, Kista, Sweden, precision 1 $\mu$m) by taking the average of five measurements. The WVTR and water vapor permeability (WVP) were calculated using the equations below

$$\mathrm{WVTR} = (\Delta W/t)/A;\ \mathrm{WVP} = \mathrm{WVTR}^{*}l/(P_{\mathrm{sat}}{}^{*}\Delta\mathrm{RH})$$

where $\Delta W$ is the weight gain, $t$ is the time, $A$ is the exposed surface area of the sample, $l$ is the sample thickness, $P_{sat}$ is the saturated vapor pressure of water at 23 °C, and ΔRH is the relative humidity gradient over the sample (75%).

*Oxygen Transmission Rate (OTR).* OTR was tested using a Systech Illinois 8001 Oxygen Permeation analyzer (IL) according to ASTM D 3985-05. A mask (A Systech Illinois 8001 accessory) was used to decrease the sample surface area to 5 $cm^2$ due to sample size limitation. The pressure gradient was maintained at 1 atm, temperature was set to 23 °C, and the relative humidity of both gases ($N_2$ and $O_2$) was 50%. Two replicates of each sample were measured. Oxygen permeation (OP) was calculated from the OTR result using the equation below.

$$\mathrm{OP} = \mathrm{OTR}^{*}(l/\Delta P)$$

where $l$ is the thickness of the sample and $\Delta P$ is the pressure gradient.

*UV Transmittance.* The UV transmittance of the LCNF films was measured with at least six technical replicates by a Shimadzu UV 2600 spectrophotometer with ISR-2600 Plus integrating sphere attachment in the wavelength range between 290 and 400 nm.

*NMR Spectroscopy.* Solid-state $^{13}C$ cross polarized magic angle spinning (CP/MAS) NMR spectra were measured using Bruker Avance III spectrometer operating at 500 MHz for protons using a double-resonance CP/MAS probehead. Samples were packed into 4 mm OD $ZrO_2$ rotors and plugged with KEL-F endcaps and spun at a spinning frequency of 8 kHz. The length of the contact time for cross-polarization was 1 ms, and a variable-amplitude cross-polarization ramped from 70 to 100% amplitude during the contact time. During the acquisition period, the protons were decoupled using SPINAL-64 decoupling and the length of the acquisition was 27 ms. At least 3000 scans were collected with a 5 s relaxation delay and the spectra were externally referenced to adamantane. $^{1}H$ NMR, $^{13}C$ NMR, and phase-sensitive two-dimensional (2D) $^{1}H-^{13}C$ heteronuclear single quantum coherence (HSQC) spectra were acquired using dimethyl sulfoxide (DMSO)/pyridine (4:1) as the solvent[23] at 22 °C and a 400 MHz Bruker Avance III spectrometer. 1,3,5-Trioxane ($\delta$C 93.1, $\delta$H 5.12 ppm) and DMSO ($\delta$C 39.5, $\delta$H 2.49 ppm) were used as internal standards for chemical shift calibration. NMR data was interpreted


https://dx.doi.org/10.1021/acsanm.1c00071
ACS Appl. Nano Mater. 2021, 4, 2921−2929

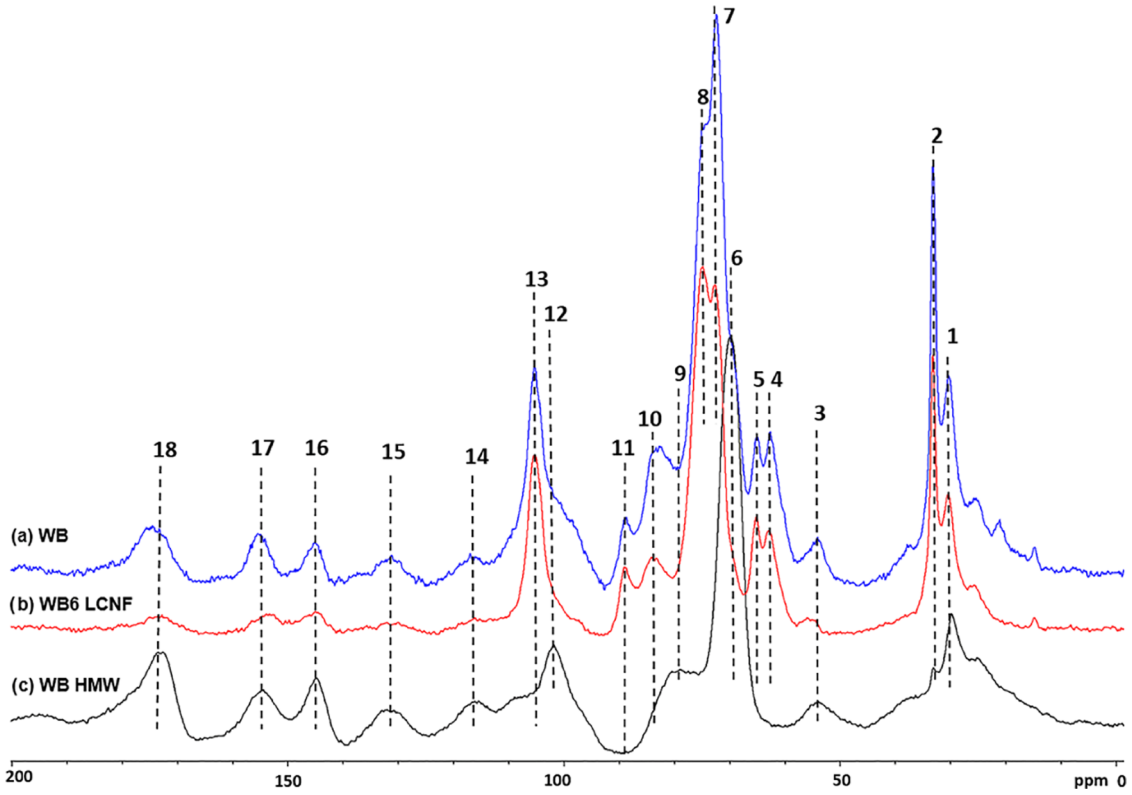


**Figure 2.** Solid-state $^{13}C$ CP/MAS spectra of (a) the willow bark; (b) LCNF from WB; and (c) dissolved HMW fraction after treating WB with aqueous 60% *p*-TsOH. Abbreviations: see caption to Table 1. Label numbers: see caption to Table S3.

using TopSpin 3.0 software and image contours were colorized in an Adobe Illustrator. The detailed experimental parameters were similar to those in the previous work.[24] The contents of hydroxyl and carboxylic acid groups were analyzed by quantitative $^{31}P$ NMR spectroscopy.[25] The HMW was dried in a vacuum oven overnight at 40 °C prior to phosphitylation using 2-chloro-4,4,5,5-tetramethyl-1,3,2-dioxaphospholane (TMDP) and measured as described previously[26] except that the relaxation delay d1 of 5 s was set here. The reported values are the mean values of two independent experiments.

High performance size-exclusion chromatography (HP-SEC): The HP-SEC system employed a series of three PSS MCX 5 $\mu$m 300 mm × 8 mm 100, 500, and 1000 Å columns eluted with aqueous 0.1 M NaOH at 30 °C. A variable-wavelength detector set at 280 nm was used to monitor the effluent. $M_n$ and $M_w$ were calculated from a linear calibration curve constructed with narrow-polydispersity polystyrene sulfonate (sodium salt) standards. The samples were first stirred for a few hours at 23 °C and then filtered through a 0.45 $\mu$m membrane prior to analysis on the same day.

## RESULTS AND DISCUSSION

**Chemical Composition of LCNF.** Figure S2 and Table S1 summarize the chemical compositions of willow bark (WB), hot water-extracted willow bark (HWEWB), and lignin-containing nanofibrils (LCNF) obtained from these after *p*-TsOH treatment. The yield loss in the pepsin treatment of WB and HWEWB was >10%, indicating that the protein content of the original bark was high (Table 1). In contrast, the pepsin treatment of LCNFs resulted in small yield losses, which showed that the *p*-TsOH treatment solubilized the proteins.[27] The Klason lignin content of WB (17.3 ± 0.7%), determined after the pepsin treatment, was lower than the previously reported value (24.7 ± 0.1%)[28] due to the pepsin treatment, which indicates that the acid-insoluble lignin content of the bark has been frequently overestimated due to interfering proteins.[29] The mass balance of Klason lignin (Table 1) revealed that hardly any lignin was solubilized in the *p*-TsOH treatment, which may explain its reported high thermal stability of the willow bark-derived LCNF from similar treatment.[18]

Although the LCNF yield was 12% higher from HWEWB than from WB, the overall yields, considering the yield loss in hot water extraction of WB, were comparable. Interestingly, the captured willow bark (Karin hybrid) water extracts[30] are shown to be effective against some specific treaths. Picein, the major bioactive component in the Karin bark water extracts,[30] has a significant role in suppressing the menadione (vitamin K precursor) induced oxidative stress effects on the mitochondrial integrity in neuroblastoma cells.[31] Triandrin acts as a stress-response modifier in regulating plant adaptogenic activity.[32] Furthermore, picein and triandrin can be chromatographically recovered[33] for possible pharmaceutical use.

The main differences between the $^{13}C$ CP/MAS NMR spectra of the two types of LCNFs were in their signal intensities. The prior hot water extraction increased the pectin yield as indicated by the higher signal intensities at ca. 173, 102 (shoulder), and 70 ppm, all characteristic of polygalacturonic acid (Figures 2, S3, and S4). Obviously, some structural modification of the pectins during the hot water treatment stabilized them against the *p*-TsOH treatment. A partial demethylation reaction could be the reason for the stabilization because the ratio of the methoxyl (54 ppm) and carboxyl (173 ppm) signals of LCNF was significantly lower when WB was extracted with hot water after the *p*-TsOH treatment (Figures S3 and S4). On the other hand, the same ratio was larger in the dissolved HMW fraction, which may show a correlation


https://dx.doi.org/10.1021/acsanm.1c00071
ACS Appl. Nano Mater. 2021, 4, 2921−2929

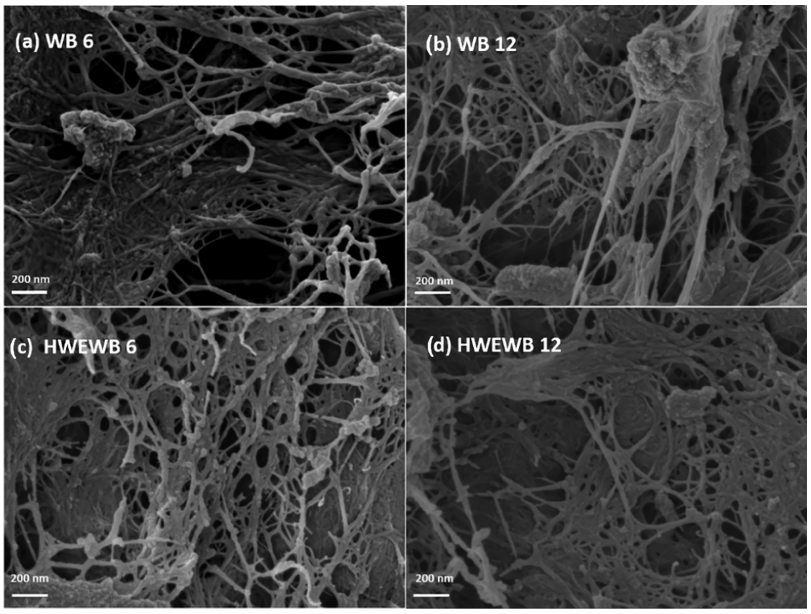


**Figure 3.** SEM images of freeze-dried LCNFs prepared from *p*-TsOH-treated willow bark (WB) and hot water-extracted willow bark (HWEWB) under 6 and 12 cycles of microfluidization: (a) WB 6; (b) WB 12; (c) HWEWB 6; and (d) HWEWB 12.

between the degree of methylation and solubilization of pectins in this case. In line with the aforementioned observations, the hot water pretreatment decreased the pectin content[34] and the amount of HMW fraction of the dissolved material from the *p*-TsOH treatment (Table S2 and Figure S5). On the other hand, the disappearance of arabinose, rhamnose, and galactose signals clearly showed removal of the neutral components of pectin (Figure S2).

The $^{13}$C CP/MAS NMR spectra of WB, HWEWB, LCNFs, and the HMW fractions all had similar aromatic/unsaturated bands at 116, 131, 145, and 155 ppm although the signal intensities were lower in LCNF compared with WB (Figures 2 and S3–S5). The HMW fractions had an additional signal at ca. 109 ppm that was earlier assigned to a condensation product of WB's aromatic substances and hydroxymethylfurfural (HMF) formed from fructose under harsh acidic conditions (Figures 2 and S5).[30,35] Furthermore, strong and sharp aliphatic carbon resonances (30 and 33 ppm) were present in WB and LCNFs made from it and HWEWB (Figures 2, S3–S5, and Table S3). One of these bands (30 ppm) was present also in the spectra of the dissolved HMW fractions, which shows that the aliphatic substances, most probably suberin,[36] were partially solubilized by the *p*-TsOH treatment. The hot water pretreatment seemed to lead to a lower aliphatic carbon content in LCNFs and a higher content in HMW (Table S4). Additional information on the HMW fractions is reported under Supporting Information (Tables S5–S7 and Figures S6–S8).

**Fibril Morphology.** SEM imaging was used to visualize the morphological structure of freeze-dried LCNFs (Figures 3 and S9–S12). In addition to thin fibrils, the precipitates or particles of variable size that we observed in the fibril network seem to be larger in WB LCNF than in HWEWB LCNF although the differences are negligible. The mean fibril thickness, measured by AFM image analysis of the LCNF films, was 26 nm (Figure S13). A similar value was reported earlier[18] for fibrils obtained after 30 min milling of *p*-TsOH-treated willow bark with a super mass colloider.

**Film Barrier Properties.** The hydrophobicity of the LCNF films was evaluated based on the water contact angle (WCA) and surface roughness. Willow bark LCNF films had hydrophobic surfaces with WCA values in the range of 107–116° (Table 2 and Figure S14). Furthermore, the surface roughness also contributed to the hydrophobicity of the films (Figure S15 and Table 2). Interestingly, WB 12 stood out possibly as the most hydrophobic among the studied films for featuring highest WCA and lowest surface roughness parameters from both $R_q$ and $R_a$. In general, the LCNF films made of WB were more hydrophobic than the films made of HWEWB. One possible explanation for this can be derived from the $^{13}$C CP/MAS spectra of the LCNF films (Figures S3 and S4) that showed significant resonance bands at 30 and 33 ppm, which were tentatively assigned for the aliphatic suberin hydrocarbons. Hence, the hypothesis is that suberin contributes more to the hydrophobicity than residual lignin does as WB 12 has the highest aliphatic hydrocarbon content among all LCNF films (Table S4). Moreover, WB 12 exhibited the highest tensile index and breaking strain among them (Table S8). The hydrophobicity and presence of lignin[37] seem to have some effect on the mechanical properties of the LCNF films; a similar observation was also reported earlier.[18] The appearance

**Table 2. Surface Roughness Parameters ($R_q$ and $R_a$) and Water Contact Angle of LCNF Films**[a]

| sample | $R_q$ (nm) | $R_a$ (nm) | *n* | water contact angle (°) |
|---|---|---|---|---|
| WB 6 | 14.6 ± 2.1 | 10.1 ± 2.9 | 2 | 110 ± 7 |
| WB 12 | 1.0 ± 0.2 | 0.73 ± 0.03 | 2 | 116 ± 4 |
| HWE WB 6 | 27.3 ± 3.7 | 21.2 ± 2.2 | 3 | 107 ± 2 |
| HWE WB 12 | 13.1 ± 3.9 | 10.2 ± 3.3 | 3 | 108 ± 3 |

[a] *n* refers to the number of analyzed images for roughness parameters. $R_q$ is the root mean square and is defined as the standard deviation of the surface height distribution. $R_a$ is the average height parameter, which is defined as the average absolute deviation of the roughness from a mean line.



https://dx.doi.org/10.1021/acsanm.1c00071
ACS Appl. Nano Mater. 2021, 4, 2921–2929

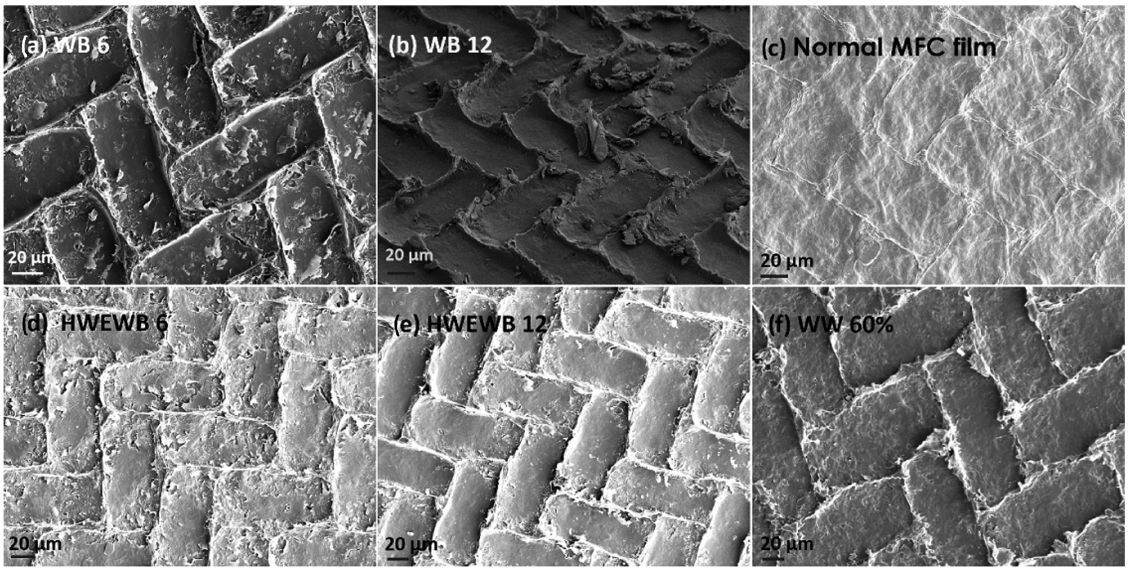


**Figure 4.** SEM images of the LCNF films of *p*-TsOH-treated willow bark (WB) and hot water-extracted willow bark (HWEWB) after 6 and 12 cycles of microfluidization in comparison with the MFC film of softwood kraft pulp and willow wood LCNF film:[18] (a) WB 6; (b) WB 12; (c) MFC (softwood kraft pulp); (d) HWEWB 6; (e) HWEWB 12; and (f) willow wood after fractionation with 60% *p*-TsOH.

**Table 3. Water Vapor Transmission Rate (WVTR), Water Vapor Permeability (WVP), Oxygen Transmission Rate (OTR), and Oxygen Permeability (OP) of the LCNF Films Produced from Willow Bark (WB) and Hot Water Extracted Willow Bark (HWEWB) after Treatment with *p*-Toluenesulfonic Acid**

| | water vapor barrier | | | oxygen barrier | | |
|---|---|---|---|---|---|---|
| | thickness μm | WVTR g/m$^2$·day | WVP g·mm/m$^2$kPa·day | Thickness μm | OTR cm$^3$/m$^2$·day | OP cm$^3$·μm/m$^2$·kPa·day |
| WB 6 | 68 ± 9 | 227 ± 19 | 7.1 ± 0.3 | 63 ± 4 | 20.0 ± 5.7 | 12.0 ± 2.8 |
| WB 12 | 77 ± 3 | 170 ± 7 | 6.0 ± 0.1 | 73 ± 8 | 10.5 ± 4.1 | 7.4 ± 2.1 |
| HWEWB 6 | 83 ± 4 | 125 ± 5 | 4.8 ± 0.2 | 83 ± 1 | 3.8 ± 0.1 | 3.1 ± 0.0 |
| HWEWB 12 | 79 ± 4 | 134 ± 6 | 4.9 ± 0.4 | 74 ± 2 | 3.6 ± 0.4 | 2.7 ± 0.2 |

of the fluffy flakes and rectangular-shaped structures that can be seen in Figures 4 and S16–S20 possibly originates from the outer bark of the willow and the polyamine monofilament mesh, respectively. In comparison, the MFC film of softwood kraft pulp had a more homogeneous surface structure, while the LCNF made of willow wood through a *p*-TsOH treatment reproduced the mesh structure of the support.[18]

The low oxygen permeability values of the willow bark LCNF films (Table 3) demonstrate their excellent oxygen barrier performance. In particular, the HWEWB LCNF films achieved an oxygen permeability of 2.6–3.1 cm$^3$·μm/m$^2$·kPa·day under 50% relative humidity, which is among the lowest ones reported for pure bio-based[38] and commercial synthetic materials[39] and is also comparable to that of covalently functionalized nanocellulose and nanocrystal films (Table 4).[14,15,40] The HWEWB LCNF films showed a lower permeability for both oxygen and water vapor than the films prepared from the bark without the hot water extraction pretreatment. Low-molecular-weight compounds, such as extractives[41] and polyphenols,[42,43] have been speculated to contribute to the plasticization and consolidation of polymer and nanocellulose films. Suberin was reported not only to limit the oxygen diffusion process in willow trees as an adaptation to the flooding environment where willow traditionally grow[44] but also to improve the hydrophobicity of the lignocellulosic fiber network.[45] Thus, the permeation of oxygen and water vapor is a complex phenomenon and it is difficult to specify the reasons for the observed behavior. The degree of crystallinity and the crystalline features of these films may explain their barrier performances. These are beyond the scope of this study.

**Table 4. Oxygen Permeability (cm$^3$·μm/m$^2$·kPa·day) of HWEWB LCNF Films in Comparison with Literature Values Reported for Other Bio-Based and Synthetic Films[a]**

| film type | sample description | oxygen permeability |
|---|---|---|
| present work | HWE willow bark LCNF films | 2.6–3.1 |
| cellulose-based | reductive amination with taurine nanocellulose[14] | 0.44 ± 0.07 |
| | *tert*-butylamino-functionalized cellulose nanocrystal film[15] | 0.25 ± 0.07 |
| | oxidized cellulose nanofibrils in sodium form[40] | 2.5 |
| | oxidized cellulose nanofibrils in protonated form[40] | 6.9 |
| starch-based[38] | amylose | 7 |
| | amylopectin | 14 |
| protein-based[39] | whey protein with glycerol (2.3:1) | 76.1 |
| | whey protein with sorbitol (2.3:1) | 4.3 |
| synthetic[39] | polyvinylidene chloride | 0.4–5.1 |
| | polyester | 15.6 |
| | high-density polyethylene | 427 |

[a]All the values were measured at 23 °C and 50% relative humidity similar to the present study.

Inspired by the inherent dark color of the willow bark LCNF films, their UV light-blocking ability was characterized using a


https://dx.doi.org/10.1021/acsanm.1c00071
ACS Appl. Nano Mater. 2021, 4, 2921–2929

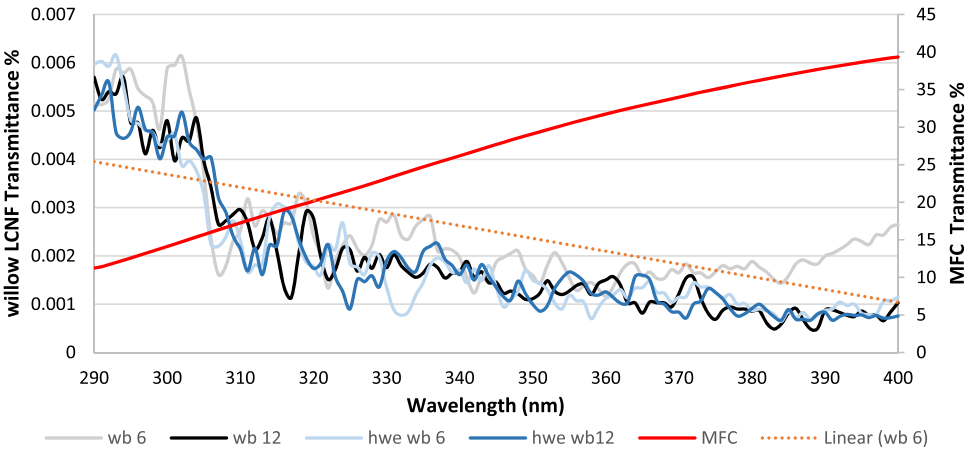


**Figure 5.** UV−vis transmission spectra of LCNF films produced from willow bark (WB) and hot water-extracted willow bark (HWEWB) in comparison with an MFC film of bleached kraft pulp in the wavelength range of 290−400 nm.

spectrophotometer equipped with an integrating sphere. These films were not optically transparent at visible wavelengths. All the films filtered 99.99−99.999% of the UV light at 290−400 nm (Figure 5 and Table S9). This protection is much higher than what could be achieved with LCNF films made of unbleached kraft pulps, not to mention MFC films of bleached kraft pulps. The UV light-absorbing structures in WB and HWEWB originate from lignin and other polyphenols[46,47] that undergo different dehydration and condensation reactions under the acidic conditions of the *p*-TsOH treatment.

## CONCLUSIONS

Natural functional and hydrophobic films of lignin-containing nanofibrils (LCNF) were prepared from willow bark (WB) by treatment with aqueous *p*-toluenesulfonic acid (*p*-TsOH). The treatment modified the structure of lignin and other polyphenolic substances of WB and solubilized them partly. Almost no Klason lignin was dissolved in the *p*-TsOH treatment. Additionally, WB LCNFs had a high suberin content and a low surface roughness, which obviously was a major reason for the hydrophobicity. WB LCNF films had an excellent oxygen barrier and UV protection properties. Pre-extraction of WB prior to the *p*-TsOH treatment made the LCNF films less permeable to oxygen gas and water vapor. These or similar nanocellulose films could potentially be utilized in sandwich barrier layers, mitigating the photo-induced oxidation in food packaging. The LCNF film preparation could be integrated with recovery of valuable water extracts of WB for its full utilization.

## ASSOCIATED CONTENT

### Supporting Information

The Supporting Information is available free of charge at https://pubs.acs.org/doi/10.1021/acsanm.1c00071.

Analytical process scheme for preparing samples for chemical composition analysis from willow bark and HWEWB together with their fibril samples; overall chemical composition and carbohydrate composition of the experimental samples; solid-state $^{13}C$ CP/MAS spectrum of the LCNF fibrils and its associated HMW; HSQC NMR spectra of the dissolved and precipitated HMW fraction in comparison with the enzymatically isolated Karin bark lignin; SEM images of the associated LCNF films; the water contact angle images show the shape of water droplets on the LCNF fibril networks and films; quantitative AFM measurements illustrating the height image of the studied fibrils; ultraviolet (UV) transmittance of the produced LCNF films (PDF)

## AUTHOR INFORMATION


### Corresponding Author

**Jinze Dou** − *Department of Bioproducts and Biosystems, Aalto University, Espoo FI-02150, Finland;* orcid.org/0000-0001-8782-3381; Email: jinze.dou@aalto.fi

### Authors

**Tapani Vuorinen** − *Department of Bioproducts and Biosystems, Aalto University, Espoo FI-02150, Finland;* orcid.org/0000-0002-5865-1776

**Hanna Koivula** − *Department of Food and Nutrition, University of Helsinki, Helsinki FI-00014, Finland*

**Nina Forsman** − *Department of Bioproducts and Biosystems, Aalto University, Espoo FI-02150, Finland*

**Mika Sipponen** − *Department of Bioproducts and Biosystems, Aalto University, Espoo FI-02150, Finland;* orcid.org/0000-0001-7747-9310

**Sami Hietala** − *Department of Chemistry, University of Helsinki, Helsinki FI-00014, Finland;* orcid.org/0000-0003-1448-1813

Complete contact information is available at: https://pubs.acs.org/10.1021/acsanm.1c00071


### Notes

The authors declare no competing financial interest.

## ACKNOWLEDGMENTS

This work made use of the Aalto University Nanomicroscopy Center (Aalto-NMC) premises. The authors thank Ting Guan from Aalto University for her skillful assistance in the initial phase of the experimental development. Appreciation is also extended to Rita Hatakka and Tuyen Nguyen for their assistance with the HPAEC analysis and microfluidizer operation. This work was a part of the Academy of Finland's Flagship Programme under Projects Nos. 318890 and 318891 (Competence Center for Materials Bioeconomy, FinnCERES).



https://dx.doi.org/10.1021/acsanm.1c00071
ACS Appl. Nano Mater. 2021, 4, 2921−2929

## REFERENCES


(1) Rutten, M. M. What economic theory tells us about the impacts of reducing food losses and/or waste: implications for research, policy and practice. *Agric. Food Secur.* **2013**, *2*, 1−13.

(2) Wang, J.; Gardner, D. J.; Stark, N. M.; Bousfield, D. W.; Tajvidi, M.; Cai, Z. Moisture and Oxygen Barrier Properties of Cellulose Nanomaterial-Based Films. *ACS Sustainable Chem. Eng.* **2018**, *6*, 49−70.

(3) Choe, E.; Min, D. B. Chemistry and Reactions of Reactive Oxygen Species in Foods. *Crit. Rev. Food Sci. Nutr.* **2006**, *46*, 1−22.

(4) Kwon, S.; Orsuwan, A.; Bumbudsanpharoke, N.; Yoon, C.; Choi, J.; Ko, S. A Short Review of Light Barrier Materials for Food and Beverage Packaging. *Korean J. Packag. Sci. Technol.* **2018**, *24*, 141−148.

(5) Cardoso, D. R.; Libardi, S. H.; Skibsted, L. H. Riboflavin as a Photosensitizer. Effects on human Health and Food Quality. *Food Funct.* **2012**, *3*, 487−502.

(6) Majdi, M.; Milani, B. Y.; Movahedan, A.; Wasielewski, L.; Djalilian, A. R. The Role of Ultraviolet Radiation in the Ocular System of Mammals. *Photonics* **2014**, *1*, 347−368.

(7) Ferrer, A.; Pal, L.; Hubbe, M. Nanocellulose in packaging: Advances in barrier layer technologies. *Ind. Crops Prod.* **2017**, *95*, 574−582.

(8) Jiang, Y.; Song, Y.; Miao, M.; Cao, S.; Feng, X.; Fang, J.; Shi, L. Transparent nanocellulose hybrid films functionalized with ZnO nanostructures for UV-blocking. *J. Mater. Chem. C* **2015**, *3*, 6717−6724.

(9) Nouri, L.; Nafchi, A. M. Antibacterial, mechanical, and barrier properties of sago starch film incorporated with betel leaves extract. *Int. J. Biol. Macromol.* **2014**, *66*, 254−259.

(10) Begley, T. H.; Biles, J. E.; Cunningham, C.; Piringer, O. Migration of a UV stabilizer from polyethylene terephthalate (PET) into food simulants. *Food Addit. Contam.* **2004**, *21*, 1007−1014.

(11) Skocaj, M.; Filipic, M.; Petkovic, J.; Novak, S. Titanium dioxide in our everyday life; is it safe? *Radiol. Oncol.* **2011**, *45*, 227−247.

(12) Yousif, E.; Haddad, R. Photodegradation and photostabilization of polymers, especially polystyrene: review. *SpringerPlus* **2013**, *2*, No. 398.

(13) Isogai, A.; Saito, T.; Fukuzumi, H. TEMPO-oxidized cellulose nanofibers. *Nanoscale* **2011**, *3*, 71−85.

(14) Sirviö, J. A.; Kolehmainen, A.; Visanko, M.; Liimatainen, H.; Niinimäki, J.; Hormi, O. E. O. Strong, Self-Standing Oxygen Barrier Films from Nanocelluloses Modified with Regioselective Oxidative Treatments. *ACS Appl. Mater. Interfaces* **2014**, *6*, 14384−14390.

(15) Visanko, M.; Liimatainen, H.; Sirviö, J. A.; Mikkonen, K. S.; Tenkanen, M.; Sliz, R.; Hormi, O.; Niinimäki, J. Butylamino-functionalized cellulose nanocrystal films: barrier properties and mechanical strength. *RSC Adv.* **2015**, *5*, 15140−15146.

(16) Missoum, K.; Belgacem, M. N.; Bras, J. Nanofibrillated Cellulose Surface Modification: A Review. *Materials* **2013**, *6*, 1745−1766.

(17) Adudonia, K. S.; Saad, G. R.; Naguib, H. F.; Ewis, M.; Zahran, D.; Elsabee, M. Z. Surface modification of polypropylene film by grafting with vinyl monomers for the attachment of chitosan. *J. Polym. Res.* **2018**, *25*, 125.

(18) Dou, J.; Bian, H.; Yelle, D. J.; Ago, M.; Vajanto, K.; Vuorinen, T.; Zhu, J. Y. Lignin containing cellulose nanofibril production from willow bark at 80 °C using a highly recyclable acid hydrotrope. *Ind. Crops Prod.* **2019**, *129*, 15−23.

(19) Chen, L.; Dou, J.; Ma, Q.; Li, N.; Wu, R.; Bian, H.; Yelle, D. J.; Vuorinen, T.; Fu, S.; Pan, X.; Zhu, J. Rapid and near-complete dissolution of wood lignin at ≤80 °C by a recyclable acid hydrotrope. *Sci. Adv.* **2017**, *3*, No. e1701735.

(20) Rajala, S.; Siponkoski, T.; Sarlin, E.; Mettänen, M.; Vuoriluoto, M.; Pammo, A.; Juuti, J.; Rojas, O. J.; Franssila, S.; Tuukkanen, S. Cellulose Nanofibril Film as a Piezoelectric Sensor Material. *ACS Appl. Mater. Interfaces* **2016**, *8*, 15607−15614.

(21) Mendes, J. A. S.; Prozil, S. O.; Evtuguin, D. V.; Lopes, L. P. C. Towards comprehensive utilization of winemaking residues: Characterization of grape skins from red grape pomaces of variety Touriga Nacional. *Ind. Crops Prod.* **2013**, *43*, 25−32.

(22) Webb, H. K.; Truong, V. K.; Hasan, J.; Fluke, C.; Crawford, R. J.; Ivanova, E. P. Roughness Parameters for Standard Description of Surface Nanoarchitecture. *Scanning* **2012**, *34*, 257−263.

(23) Kim, H.; Ralph, J. Solution-state 2D NMR of ball-milled plant cell wall gels in DMSO-$d_6$/pyridine-$d_5$. *Org. Biomol. Chem.* **2010**, *8*, 576−591.

(24) Dou, J.; Paltakari, J.; Johansson, L.; Vuorinen, T. Novel Insight into the Separation and Composite Utilization of Sclerenchyma Fiber Bundles of Willow Bark. *ACS Sustainable Chem. Eng.* **2019**, *7*, 2964−2970.

(25) Granata, A.; Argyropoulos, D. S. 2-Chloro-4,4,5,5-tetramethyl-1,3,2-dioxaphospholane, a Reagent for the Accurate Determination of the Uncondensed and Condensed Phenolic Moieties in Lignins. *J. Agric. Food Chem.* **1995**, *43*, 1538−1544.

(26) Sipponen, M. H.; Smyth, M.; Leskinen, T.; Johansson, L.; Österberg, M. All-lignin approach to prepare cationic colloidal lignin particles: stabilization of durable Pickering emulsions. *Green Chem.* **2017**, *19*, 5831−5840.

(27) Liu, T. Y.; Chang, Y. H. Hydrolysis of proteins with *p*-Toluenesulfonic acid. Determination of tryptophan. *J. Biol. Chem.* **1971**, *246*, 2842−2848.

(28) Dou, J.; Kim, H.; Li, Y.; Padmakshan, D.; Yue, F.; Ralph, J.; Vuorinen, T. Structural Characterization of Lignins From Willow Bark and Wood. *J. Agric. Food Chem.* **2018**, *66*, 7294−7300.

(29) Kim, H.; Padmakshan, D.; Li, Y.; Rencoret, J.; Hatfield, R. D.; Ralph, J. Characterization and Elimination of Undesirable Protein Residues in Plant Cell Wall Materials for Enhancing Lignin Analysis by Solution-State Nuclear Magnetic Resonance Spectroscopy. *Biomacromolecules* **2017**, *18*, 4184−4195.

(30) Dou, J.; Xu, W.; Koivisto, J. J.; Mobley, J. K.; Padmakshan, D.; Kögler, M.; Xu, C.; Willför, S.; Ralph, J.; Vuorinen, T. Characteristics of Hot Water Extracts from the Bark of Cultivated Willow (*Salix* sp.). *ACS Sustainable Chem. Eng.* **2018**, *6*, 5566−5573.

(31) Kesari, K. K.; Dhasmana, A.; Shandilya, S.; Prabhakar, N.; Shaukat, A.; Dou, J.; Rosenholm, J. M.; Vuorinen, T.; Ruokolainen, J. Plant-Derived Natural Biomolecule Picein Attenuates Menadione Induced Oxidative Stress on Neuroblastoma Cell Mitochondria. *Antioxidants* **2020**, *9*, No. 552.

(32) Panossian, A.; Hamm, R.; Wikman, G.; Efferth, T. Mechanism of action of Rhodiola, salidroside, tyrosol and triandrin in isolated neuroglial cells: An interactive pathway analysis of the downstream effects using RNA microarray data. *Phytomedicine* **2014**, *21*, 1325−1348.

(33) Dou, J.; Heinonen, J.; Vuorinen, T.; Xu, C.; Sainio, T. Chromatographic recovery and purification of natural phytochemicals from underappreciated willow bark water extracts. *Sep. Purif. Technol.* **2021**, *261*, No. 118247.

(34) Sinitsya, A.; Čopíková, J.; Pavlíková, H. $^{13}$C CP/MAS NMR Spectroscopy in the Analysis of Pectins. *J. Carbohydr. Chem.* **1998**, *17*, 279−292.

(35) Koch, H.; Pein, J. Condensation Reactions Between Phenol, Formaldehyde and 5-Hydroxymethylfurfural, Formed as Intermediate in the Acid Catalyzed Dehydration of Starchy Products. *Polym. Bull.* **1985**, *13*, 525−532.

(36) Lopes, M. H.; Gil, A. M.; Silvestre, A. J. D.; Neto, C. P. Composition of Suberin Extracted upon Gradual Alkaline Methanolysis of *Quercus suber* L. Cork. *J. Agric. Food Chem.* **2000**, *48*, 383−391.

(37) Rojo, E.; Peresin, M. S.; Sampson, W. W.; Hoeger, I. C.; Vartiainen, J.; Laine, J.; Rojas, O. J. Comprehensive elucidation of the effect of residual lignin on the physical, barrier, mechanical and surface properties of nanocellulose films. *Green Chem.* **2015**, *17*, 1853−1866.

(38) Rindlav-Westling, Å.; Stading, M.; Hermansson, A.; Gatenholm, P. Structure, mechanical and barrier properties of amylose and amylopectin films. *Carbohydr. Polym.* **1998**, *36*, 217−224.




https://dx.doi.org/10.1021/acsanm.1c00071
ACS Appl. Nano Mater. 2021, 4, 2921−2929

(39) Miller, K. S.; Krochta, J. M. Oxygen and aroma barrier properties of edible films: A review. *Trends Food Sci. Technol.* **1997**, *8*, 228−237.
(40) Shimizu, M.; Saito, T.; Isogai, A. Water-resistant and high oxygen-barrier nanocellulose films with interfibrillar cross-linkages formed through multivalent metal ions. *J. Membr. Sci.* **2016**, *500*, 1−7.
(41) Medina Jaramillo, C.; Seligra, P. G.; Goyanes, S.; Bernal, C.; Famá, L. Biofilms based on cassava starch containing extract of *yerba mate* as antioxidant and plasticizer. *Starch* **2015**, *67*, 780−789.
(42) Baumberger, S.; Lapierre, C.; Monties, B. Utilization of Pine Kraft Lignin in Starch Composites: Impact of Structural Heterogeneity. *J. Agric. Food Chem.* **1998**, *46*, 2234−2240.
(43) Espinosa, E.; Bascón-Villegas, I.; Rosal, A.; Pérez-Rodríguez, F.; Chinga-Carrasco, G.; Rodríguez, A. PVA/(ligno)nanocellulose biocomposite films. Effect of residual lignin content on structural, mechanical, barrier and antioxidant properties. *Int. J. Biol. Macromol.* **2019**, *141*, 197−206.
(44) De Simone, O. D.; Haase, K.; Müller, E.; Junk, W. J.; Hartmann, K.; Schreiber, L.; Schmidt, W. Apoplasmic Barriers and Oxygen Transport Properties of Hypodermal Cell Walls in Roots from Four Amazonian Tree Species. *Plant Physiol.* **2003**, *132*, 206−217.
(45) Korpinen, R. I.; Kilpeläinen, P.; Sarjala, T.; Nurmi, M.; Saloranta, P.; Holmbom, T.; Koivula, H.; Mikkonen, K. S.; Willför, S.; Saranpää, P. T. The Hydrophobicity of Lignocellulosic Fiber Network Can Be Enhanced with Suberin Fatty Acids. *Molecules* **2019**, *24*, No. 4391.
(46) Liu, X.; Wang, J.; Li, S.; Zhuang, X.; Xu, Y.; Wang, C.; Chu, F. Preparation and properties of UV-absorbent lignin graft copolymer films from lignocellulosic butanol residue. *Ind. Crops Prod.* **2014**, *52*, 633−641.
(47) Gierer, J.; Lin, S. Y. Photodegradation of lignin. A contribution to the mechanism of chromophore formation. *Sven. Papperstidn.* **1972**, *75*, 233−237.


https://dx.doi.org/10.1021/acsanm.1c00071
*ACS Appl. Nano Mater.* 2021, 4, 2921−2929